Thermal Scenario for Casson Nanofluid Transport in a Nonlinear Dual-Extending Device Experiencing Convective Heating: A Numerical Analysis

Ephesus O. Fatunmbi[1*], Samuel A. Oke[2], Olusegun A. Olaiju[3]

[1,3]Department of Mathematics and Statistics, Federal Polytechnic, Ilaro, Nigeria.
[2]Department of Mathematics, Adekunle Ajasin, University, Akungba, Nigeria.
[1*]ephesus.fatunmbi@federalpolyilaro.edu.ng, okeabayomisamuel@yahoo.com, olusegun.olaiju@federalpolyilaro.edu.ng

Abstract

The thermal behaviour of nanofluids in complex geometries and under convective heating conditions offers essential applications for designing efficient heat exchangers and cooling systems in various industrial thermal devices. Thus, this article is embarked upon to investigate the Casson nanofluid's thermal properties over a three-dimensional plate that stretches in a nonlinear bilateral direction. The thermal field is developed by incorporating the nonlinear Rosseland approximation, an internal heat source or absorption coupled with the convective heating at the boundary, Brownian motion, and thermophoresis effects. The constructed mathematical model is further scrutinized and refined into a non-dimensional version via similarity transformation quantities, while the results for the set of nonlinear equations are obtained numerically by shooting and Runge-Kutta Fehlberg techniques. The validity of the solution in this study is authenticated by comparing it with previous similar studies in the literature under some strict restrictions. The resultant effects of the dimensionless parameters that contribute to the physical analysis are communicated through various graphs. The material and power-law index parameters are found to decelerate fluid motion, but radiation, heat source, and Casson fluid terms raise the temperature profiles. Heat transmission progresses with a hike in the Prandtl number, power-law index, and heat sink, but the reverse is the case for thermophoresis and radiation terms.

Keywords: Casson nanofluid; Convective heating; Dual-Extending sheet; Thermal radiation; Thermophoresis.

Introduction

Heat transfer is an integral part of many different industrial and applied processes and is one of the most fundamental aspects of fluid flow. The efficiency and performance of fluid flow systems can only be maximised with a thorough understanding of heat transfer and its regulations. The essentials of heat transfer in fluid flow are multifaceted, as can be found across science, engineering, and technology. The impacts include improving energy efficiency, enhancing human comfort, and various industrial processes. Thus, knowledge of the thermal behaviour of complex fluids over a stretching material device is essential in various high-temperature industrial and engineering processes such as hot rolling, metallurgical activities like polymer extrusion, paper and textile production, extrusion, crystal growing, cooling elastic sheets, and so on (Zeeshan & Majeed, 2015). Owing to these benefits, Pramanik (2015) presented the Casson fluid flow in an exponentially extending sheet experiencing suction or blowing. Sreenivasulu et al. (2016) included the impact of Joule heating, thermal radiation, and viscous dissipation on such a concept.

Most fluids which are of crucial importance in engineering and industrial works are non-Newtonian in nature. These are complex and complicated fluids (e. g. slurries, lubricants, tomato jels, paints, liquid crystals, polymeric fluids, etc.) that differ from Navier Stokes model. Various models of the non-Newtonian fluids have been developed due to the impossibility of one fluids model to describe the whole properties of the non-Newtonian fluids. Among these several fluids are the Casson fluids, Jefferey, Williamson, Prandtl-Eyring, Powell-Eyring, micropolar fluids, etc. (Zubair et al., 2017; Javed and Siddiqui, 2018; Patel and Singh, 2029; Sheri, and Shamshuddin, 2019; Fatunmbi and Okoya, 2020). In this study, thermal performance of Casson fluid is investigated due to essential properties. Casson fluid has been described as one which posses a shear thinning characteristics, displays elastic solid property, exhibits a yield stress and as such, at low rate of shear stress, the viscosity assumes infinity but at high rate of shear stress, it displays Newtonian fluid nature. Owing to its application Vajravelu et al. (2016) analytically estimated a mixed convective analysis of a Casson fluid which is configured in a nonlinearly expanding vertical material device with non-constant thermal conductivity. In their estimations, the velocity and the thermal fields were found to deplete with

higher magnitudes of the power-law index. Krishna et al. (2018) debated the flow of Casson fluid along a permeable extending surface with magnetic effects using a numerical tool. It was stated in their study that the material and magnetic field terms decelerate the velocity profiles.

The orthodox heat transfer fluids which includes water, oil ethylene glycol, etc. characterise low level of thermal conductivity which is not sufficient for heat transfer in many thermal and technological devices that are relevant in todayý world. In view of this, researchers have found a better approach to enhance heat transmission using nanofluids. Nanofluids are a mixture of solid particles made of metals or metallic oxides, carbides, carbon nanotubes, etc. with a size smaller than 100 nm in a traditional fluid. This newly formed fluid has been found to improve thermal characteristics of the regular fluids and raise heat transfer that promote cooling of many thermal devices. Application includes transportation industries, the cooling of automobiles, heat exchanger, cooling of transformer, etc. (Das et al. 2018; Shit and Mandal, 2020; Fatunmbi and Okoya, 2021). Shit and Mandal (2020) engaged Buongiornoý model to build an unsteady flow of a magnetized Casson nanofluid equations with radiation, viscous dissipation and entropy generation effects. The numerical report also features heat transfer analysis and Bejan number descriptions. Omotola and Fatunmbi (2021) employed a numerical tool to assess the thermal and mass behaviour of a Casson nanofluid over a lengthening nonlinear plate with radiation, chemical reactions and Navier slip effects. The authors reported an expanded thermal boundary structure in view of Brownian and thermophoresis terms.

The above literature, however, considered a two-dimensional device where the extending sheet is unidirectional. In practical situations, and for a three-dimensional flow, the extending material device can be in dual directions. The earliest work on boundary layer flow induced by a dual-directional lengthening was reported by Wang (1984). As a result of its practical usage in engineering works, several researchers have investigated such a problem by incorporating various parameters and imposing different flow and thermal conditions (Laha et al., 1989; Liu and Anderson, 2008; Salahuddin et al., 2020; Abbas et al., 2020). Inspired by the practical applications of such a concept in various industrial and engineering operations, the current investigation aims to evaluate the thermal behaviour of a magnetised Casson fluid, which consists of tiny nanoparticles over a nonlinear dual-extending material device. The heat profile is developed on convective heating conditions coupled with a heat source or sink and radiation effects. This numerical report finds applications in high-temperature industrial and engineering operations, like metal casting, hot rolling, glass manufacturing, and other material manufacturing processes.

Formulation of the Problem and Derivation of the Governing Equations

To develop the appropriate equations that mirror the current problem, it is essential to highlight some valuable assumptions. Consider the 3D-dimensional, incompressible, steady motion of a non-Newtonian Casson fluid consisting of tiny nanoparticles over a dual-directionally extending surface. A convective thermal condition is applied to study the heat situation of the sheet with the imposition of an external magnetic field. It is hypothesised that there is internal heat generation or absorption; the microscopic particles' thermal movement and Brownian motion also occur in the flow field, but no account of the induced magnetic field or viscous dissipation is allowed. As indicated in Figure 1, the dimensions of the sheet are fixed as (x, y, z) having corresponding components of velocity specified as (U, V, W). It is believed that the dual stretching occurs in x and y axes whereas z axis is fixed normal to the leading edges. The speed of stretching in both directions, the thermal properties, and the constraints at the wall and upstream field are indicated in equation (6).

The Governing Equations

On the basis of the aforementioned assumptions in conjunction with approximation of boundary layer theory, the model equations are listed explicitly in the following equations.

$$\frac{\partial U}{\partial x} = -\frac{\partial V}{\partial y} - \frac{\partial V}{\partial y} \tag{1}$$

$$U\frac{\partial U}{\partial x} + V\frac{\partial U}{\partial y} + W\frac{\partial u}{\partial z} = \frac{1}{\rho_f}\left(1 + \frac{1}{\gamma}\right)\frac{\partial^2 U}{\partial z^2} - \frac{\sigma B^2}{\rho_f}U, \tag{2}$$

$$U\frac{\partial V}{\partial x} + V\frac{\partial V}{\partial y} + W\frac{\partial V}{\partial z} = \frac{1}{\rho_f}\left(1 + \frac{1}{\gamma}\right)\frac{\partial^2 V}{\partial z^2} - \frac{\sigma B^2}{\rho_f}V, \tag{3}$$

$$U\frac{\partial T}{\partial x}+V\frac{\partial T}{\partial y}+W\frac{\partial T}{\partial z}=\frac{k_f}{(\rho c_p)_f}\frac{\partial^2 T}{\partial y^2}+\tau\left[\frac{D_T}{T_\infty}\left(\frac{\partial T}{\partial y}\right)^2+D_B\left(\frac{\partial T}{\partial y}\frac{\partial G}{\partial y}\right)\right]+\frac{Q_t}{(\rho c_p)_f}(T-T_\infty)+\frac{16\sigma^*}{3k^*\rho c_p}\frac{\partial}{\partial y}\left(T^3\frac{\partial T}{\partial y}\right), \tag{4}$$

$$U\frac{\partial G}{\partial x}+V\frac{\partial G}{\partial y}=D_B\frac{\partial^2 G}{\partial y^2}+\frac{D_T}{T_\infty}\left(\frac{\partial^2 T}{\partial y^2}\right). \tag{5}$$

The associated situations at the boundary for Eqs.(1-5) are listed as:

$$\begin{aligned}&U(x,y,0)=U_w=a(x+y)^\delta, V(x,y,0)=V_w=b(x+y)^\delta, W(x,y,0)=0\\&-k_f\frac{\partial T}{\partial z}\Big|_{(x,y,0)}=h_t(T_f-T), G(x,y,0)=G_w\\&U\to 0, V\to 0, T\to T_\infty, G\to G_\infty, as\quad z\to\infty.\end{aligned} \tag{6}$$

For the occurrence of similarity solutions, it is essential to state that the non-uniform magnetic field $B(x)$ is expressed as (Devi and thiyagarajan, Habibi Matin et al.) $B(x)=B_0(x+y)^{\frac{\delta-1}{2}}$ where B_0 indicates the uniform magnetic field strength. Likewise, coefficient of volumetric thermal and exponential-based heat source are respectively specified as $Q_t=Q_0(x+y)^{\delta-1}$ and h_t is the heat transfer coefficient with $h_t=h_f(x+y)^{(\delta-1)/2}$ with h_f being a constant. All symbols which have been used in the flow analysis above are collated in Table 1 and are described appropriately.

Table 1: Symbols and their description as used in equations (1-6).

Symbols	Definition	Symbols	Definition
U,V,W	velocity in x,y,z directions	T	temperature
ϑ_f	kinematic viscosity	G	concentration of nanoparticles
ρ_f	fluid density	T_f	temperature at the surface
μ_f	fluid viscosity	U_w	surface velocity along x axis
k_f	thermal conductivity	V_w	surface velocity along x axis
T_∞	temperature at free stream	G_∞	concentration at the free stream
C_p	heat capacity	N_w	concentration at the surface
D_B	Brownian diffusion coefficient	D_T	thermophoretic diffusion coefficient
k^*	mean absorption coefficient	σ^*	electrical conductivity

In line with Khan et al. (2014), the similarity tools substituted into the main equations are:

$$\begin{aligned}&\eta=z\sqrt{\frac{a(x+y)^{\delta-1}}{\vartheta_f}}, U=a(x+y)^\delta f', V=a(x+y)^\delta h', \theta(\eta)=\frac{T-T_\infty}{T_f-T_\infty}\\&\phi(\eta)=\frac{G-G_\infty}{G_w-G_\infty}, W=-\sqrt{a\nu_f(x+y)^{\delta-1}}\left[\frac{\delta+1}{2}(f+h)+\frac{\delta-1}{2}\eta(f'+h')\right].\end{aligned} \tag{7}$$

Upon substituting quantities (7) into the governing Eqs. (1-5) with the boundary conditions (6), the continuity Eq. (1) becomes valid while Eqs. (2-5) yield the underlisted:

$$\left(1+\frac{1}{\gamma}\right)\frac{d^3f}{d\eta^3}+\left(\frac{\delta+1}{2}\right)(f(\eta)+h(\eta))\frac{d^2f}{d\eta^2}-\delta\left(\frac{df}{d\eta}+\frac{dh}{d\eta}\right)\frac{df}{d\eta}-M\frac{df}{d\eta}=0, \tag{8}$$

$$\left(1+\frac{1}{\gamma}\right)\frac{d^3h}{d\eta^3}+\left(\frac{\delta+1}{2}\right)(f(\eta)+h(\eta))\frac{d^2h}{d\eta^2}-\delta\left(\frac{df}{d\eta}+\frac{dh}{d\eta}\right)\frac{dh}{d\eta}-M\frac{dh}{d\eta}=0, \tag{9}$$

$$\frac{1}{Pr}[1+Nr(1+(T_\theta-1)\theta)^3]\frac{d^2\theta}{d\eta^2}+\frac{3}{Pr}[Nr(T_\theta-1)(1+(T_\theta-1)\theta)^2]\left(\frac{d\theta}{d\eta}\right)^2+\left(\frac{\delta+1}{2}\right)(f(\eta)+h(\eta))\frac{d\theta}{d\eta}+\left(Nt\left(\frac{d\theta}{d\eta}\right)^2+Nb\left(\frac{d\theta}{d\eta}\right)\left(\frac{d\phi}{d\eta}\right)\right)+Q\theta(\eta)=0, \tag{10}$$

$$\frac{d^2\phi}{d\eta^2}+\left(\frac{\delta+1}{2}\right)(f(\eta)+h(\eta))Sc\frac{d\phi}{d\eta}+\frac{Nt}{Nb}\frac{d^2\theta}{d\eta^2}=0. \tag{11}$$

With the use of the similarity variables defined in (7), the wall constraints are transformed to:

$$\begin{aligned}&\frac{df}{d\eta}-1=0,\frac{dh}{d\eta}-\lambda=0,f(\eta)=0,h(\eta)=0,\frac{d\theta}{d\eta}=-B_t(1-\theta(\eta)),\phi(\eta)-1=0\ \ at\ \ \eta=0,\\&\frac{df}{d\eta}=0,\frac{dh}{d\eta}=0,\theta(\eta)=0,\phi(\eta)=0\ \ as\ \ \eta\to\infty.\end{aligned} \tag{12}$$

The emerging physical quantities obtained from the boundary value problem (82) are the temperature ratio (T_θ), the Prandtl number (Pr), radiation (Nr), heat source/sink (Q), Schmidt number, (Sc), Brownian motion (Nb), Biot number $(B1)$, thermophoresis (Nt), magnetic field (M), stretching ratio (λ) parameters. The descriptions of each of these terms are respectively give in equation (13) as:

$$\begin{aligned}&T_\theta=\frac{T_f}{T_\infty},Pr=\frac{(\mu C_p)_f}{k_f},Nr=\frac{16\sigma^*T_\infty^3}{3k^*k_\infty},Q=\frac{Q_0}{a\rho C_p},Sc=\frac{\nu}{D_B},Nb=\frac{D_B\tau(G_w-G_\infty)}{\vartheta_f},\\&B_t=\frac{h_f}{k_f}\sqrt{\frac{v_f}{a}},Nt=\frac{D_T\tau(T_f-T_\infty)}{T_\infty\vartheta_f},M=\frac{\sigma B_0^2}{a\rho_f},\lambda=\frac{b}{a}.\end{aligned} \tag{13}$$

The relevant quantities of engineering delight namely; coefficient of viscous drag C_{fx}, the local Nusselt number Nux and the local Sherwood number S_{hx}. The respective description of each of these quantities are

$$C_{fx}=\frac{\tau_{wx}}{\rho U_w^2},C_{fy}=\frac{\tau_{wy}}{\rho V_w^2},Nu=\frac{(x+y)q_w}{k_f(T_f-T_\infty)},S_{hx}=\frac{(x+y)q_m}{D_B(G-G_\infty)}. \tag{14}$$

In equation (14), τ_{wx} is the shear stress in x direction, τ_{wy} is the shear stress in y direction, q_w is the heat flux while q_m is the surface mass flux. The respective variables defining each of these are listed as

$$\begin{aligned}&\tau_{wx}=\mu_f\left(1+\frac{1}{\gamma}\right)\frac{\partial U}{\partial z}\Big|_{z=0},\tau_{wy}=\mu_f\left(1+\frac{1}{\gamma}\right)\frac{\partial V}{\partial z}\Big|_{z=0},q_w=-\left(k_f+\frac{16T^3\sigma}{3k^*}\right)\frac{\partial T}{\partial y}\Big|_{z=0}\\&q_m=-D_B\left(\frac{\partial G}{\partial y}\right)\Big|_{z=0}.\end{aligned} \tag{15}$$

By incorporating equations (7) and (15), the non-dimensional quantities in (14) simply transform (16-19).

$$C_{fx}=\left(1+\frac{1}{\gamma}\right)Re_x^{-1/2}\frac{d^2f}{d\eta^2}\Big|_{\eta=0}, \tag{16}$$

$$C_{fy}=\left(1+\frac{1}{\gamma}\right)Re_y^{-1/2}\frac{d^2h}{d\eta^2}\Big|_{\eta=0}, \tag{17}$$

$$Nu=-[1+Nr(1+(T_\theta-1)\theta(0))^3]Re_x^{1/2}\frac{d\theta}{d\eta}\Big|_{\eta=0}, \tag{18}$$

$$S_h=-Re_x^{\frac{1}{2}}\frac{d\phi}{d\eta}\Big|_{\eta=0}. \tag{19}$$

Solution methodology

The boundary value problem that describes the current investigations is highly nonlinear in nature, and thus, the

closed-form solution is difficult to assess, as such, a numerical solution is sought for the problem. Thus, equations (8̈1) associated with the wall conditions (12) are tackled with the shooting technique together with the Runge-Kutta Fehlberg method for the provision of the solution to the current problem. This method has been described as unconditionally stable and having high accuracy in dealing with nonlinear differential equations. The description of this method can be found in Khan et al. (2015), and it is very popular and maintains comparable efficiency to other numerical methods, such as finite elements and spectral methods. Its description is not publicized in this study due to its popularity. For the computations, the following set of values are used as default after careful selection from previous studies: $\delta = 0.5, \gamma = 0.3, M = 0.3 = Nt, B1 = Nb = Q = 0.2, Nr = 0.5, T_\theta = 1.5, Sc = 0.62$ and $Pr = 1.2$. However, to show the impact of the emerging physical terms on the non-dimensional quantities of velocity, temperature, wall frictional drag, and the Nusselt number, different graphs are assigned various values for the emerging parameters.

Results Validation

The authenticity of the derived numerical results is verified through the comparison of C_{fx} and C_{fy} values for variations in δ and λ with data reported by Khan et al. (2015) under some strict limiting conditions. As noted in Table 2, the comparison reveals a high correlation between the results obtained in the present work and previous data in the literature.

Table 2: Values of $-f''(0)$ and $-g''(0)$ for variations in δ and λ as compared with Khan et al. (2015)

		Khan et al. *(2015)*		Present results	
δ	λ	$-f''(0)$	$-g''(0)$	$-f''(0)$	$-g''(0)$
1.0	0.0	1.000000	0.00000	1.0000000	0.0000000
1.5	0.5	1.224745	0.612372	1.2252595	0.6126298
1.0	1.0	1.414214	1.414214	1.4144335	1.4144335
3.0	0.0	1.6243156	0.000000	1.6245406	0.0000000
3.0	0.5	1.989422	0.994711	1.9894627	0.9947314
3.0	1.0	2.297186	2.297186	2.2971913	2.2971913

RESULTS AND DISCUSSION

For further investigation and understanding of the behaviour of the physical quantities, various graphs have been plotted to showcase the trend of the velocity, temperature, and other quantities of engineering interest. These graphs have been grouped under different subsections as follows:

Velocity profiles versus η for variation in some parameters

Figures 2 revealed how the velocity profiles react to changes in the Casson fluid term γ and the power law exponent δ in both directions. To be precise, figures 2 and 3 elucidate clearly that the hydrodynamic boundary layer diminishes as γ escalates in the range $0.2 \leq \gamma \leq 0.8$ and such a behaviour compels a reduction in the velocity profiles as found in this figure. It is important to note that higher values of γ cause the fluid to behave like a Newtonian fluid. An increase in γ raises the dynamic viscosity of the fluid, and as such, there is a deceleration in the motion. These trends are similar in both directions and satisfy the set boundary conditions for each direction. Furthermore, figures 4 and 5 shed more light on the velocity fields in both directions as the power law exponent term δ changes in magnitude. This parameter determines the nonlinearity of the stretching velocity of the sheet at the surface. It is noted that an upsurge in the values of δ shrinks the hydrodynamic boundary layer leading to a decreasing fluid motion in both directions.

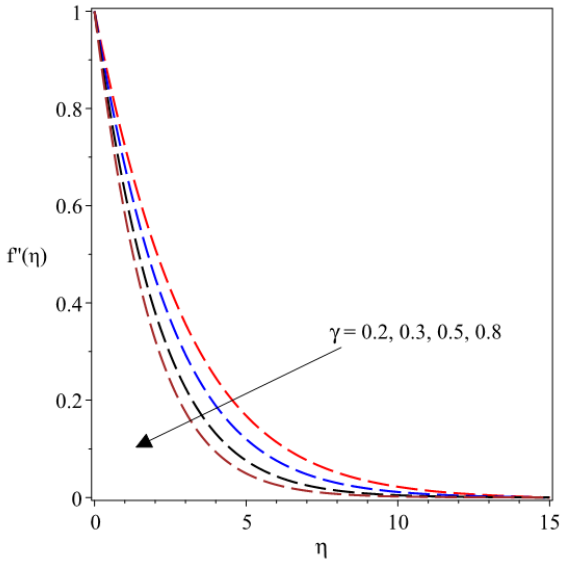

Figure 2 Graph of velocity in x direction for γ

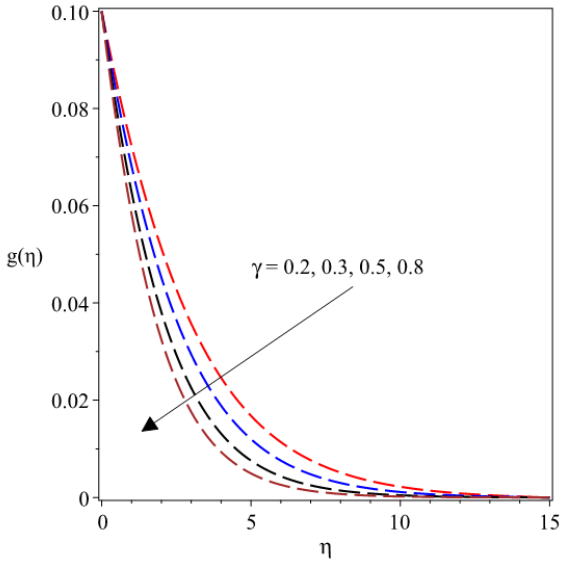

Figure 3 Trend of velocity in y direction for γ

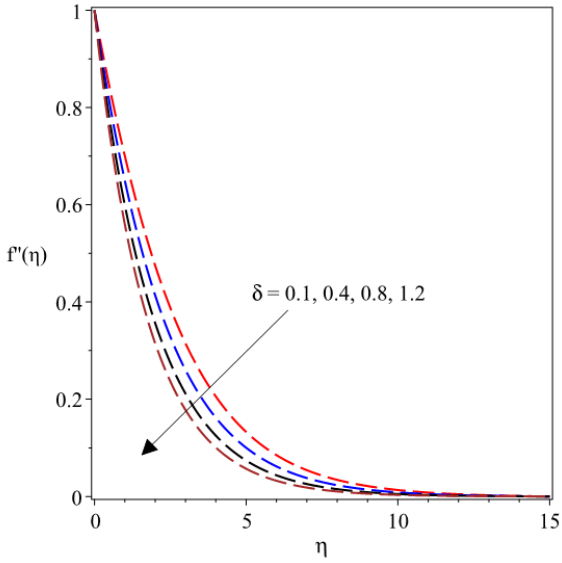

Figure 4 Velocity pattern in x direction for δ

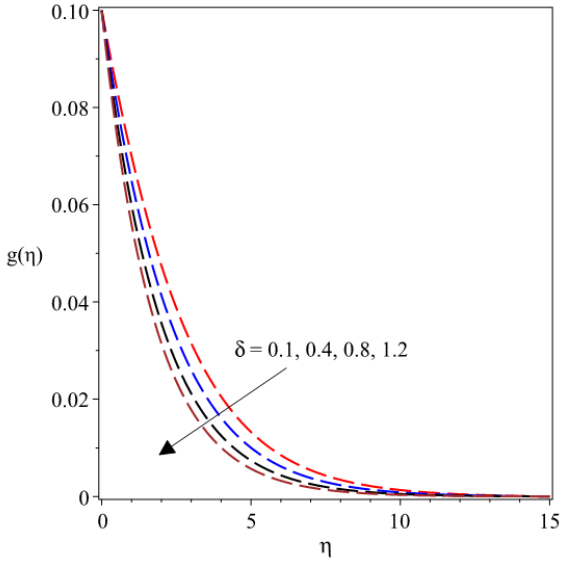

Figure 5 Velocity pattern in x direction for δ

4.2 Temperature profiles versus η for variation in some parameters

The physical nature of γ as it relates to the thermal environment is depicted in figure 6. Escalating the magnitude of γ in the interval $0.2 \leq \gamma \leq 0.8$ leads to expansion in the thermal boundary structure and, thus, a rise in the temperature profiles. The physical reason for this kind of behaviour is that the Casson nanofluid temperature gets induced as a result of the high viscosity, which creates friction in the flow field. On the other hand, there is a decrease in the thermal field as δ escalates in magnitude in the range of $0.1 \leq \delta \leq 1.2$ as illustrated in figure 7. As shown in figure 8, the heat source term, Q is proportional to the temperature distribution of the Casson nanofluid. Growth in Q raises the thermal field, which consequently raised the temperature with the corresponding expansion of the thermal boundary layer film.

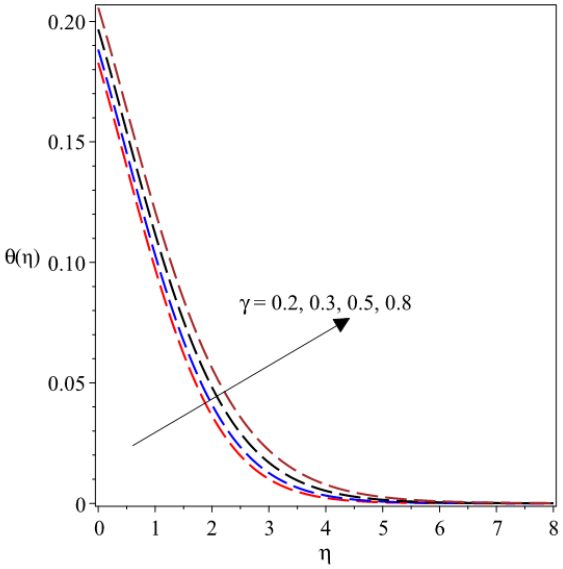

Figure 6 Thermal distribution for alteration in γ

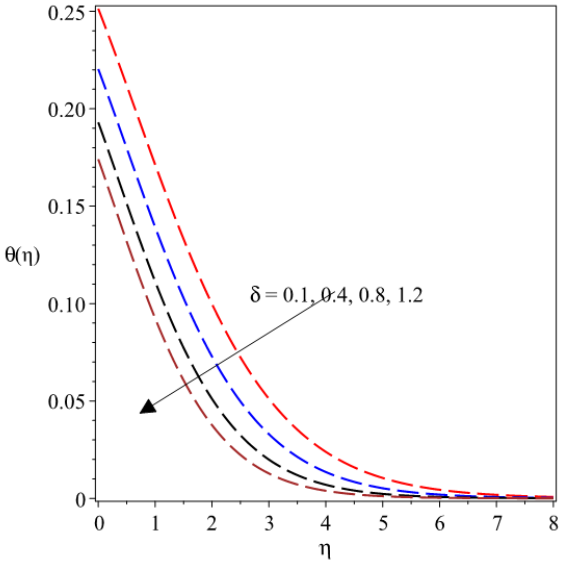

Figure 7 Thermal variation for values of δ

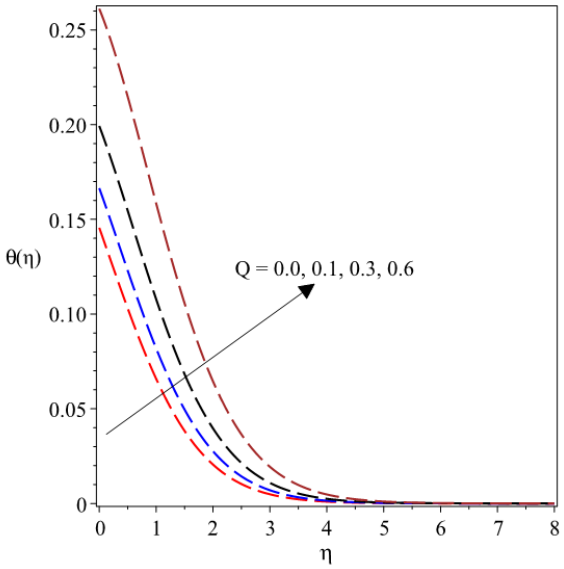

Figure 8 Thermal profiles for alteration in Q

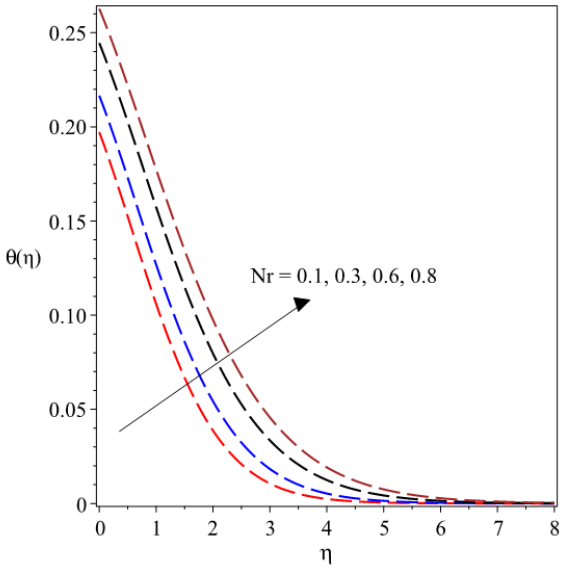

Figure 9 Thermal profiles for variations in Nr

Figure 9 reveals the trend of the thermal profiles as the radiation term Nr grows in the interval $0.1 \leq Nr \leq 0.8$. In this interval, there is a thickening of the thermal structure when Nr increases, which in turn causes a rise in the temperature of the Casson nanofluid, as noted in this figure. The temperature at the wall rises up to 0.26 and descends asymptotically to the far field region, satisfying the thermal boundary conditions.

Physical quantities of engineering variation for some parameters

Figures 10-15 describe the impact of some parameters on the physical quantities of engineering delight. Figure 10 demonstrates the nature of the viscous drag at the surface (C_{fx}) when the M, δ and γ vary in strength. The viscous drag represents the friction at the wall caused by the fluid particles and the stretching sheet. The viscous drag increases as these parameters escalate. The Lorentz force, which is induced by the transverse magnetic field, creates

more drag in the flow field and thus creates a drag to the motion of the Casson nanofluid. For linearly stretching sheet $\delta = 1$ the nature of (C_{fx}) is higher than that of nonlinearly stretching sheet $\delta = 0.5$. These trends are similar in both directions, as depicted in figures 10 and 11.

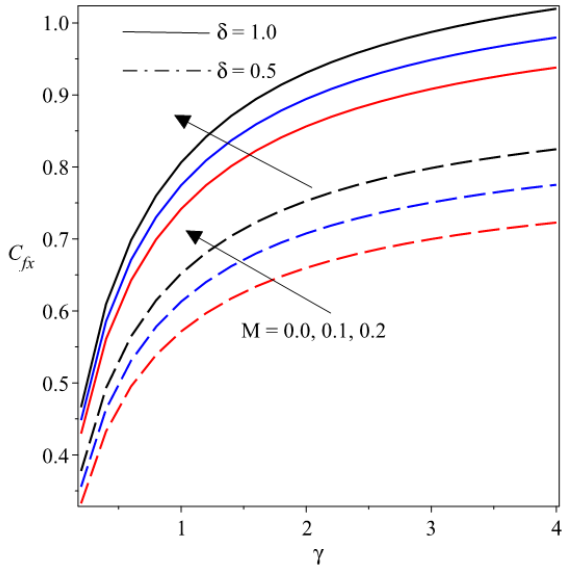

Figure 10 C_{fx} for variations in M, δ and δ

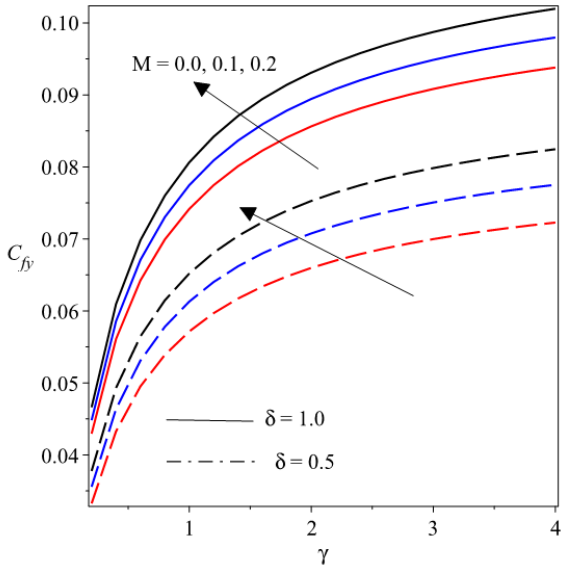

Figure 11 C_{fx} for variations in M, δ and δ

In Figure 12, the impacts of Pr, Q and Nr are checked on the heat transmission Nu_x at the sheet surface. Higher values of Pr cause an enhancement Nu_x whereas heat transfer drops with higher values of Q and Nr. Based on the definition of Pr which is the ratio of momentum to thermal diffusivity, $Pr < 1$ depicts a lesser momentum diffusion compared to the thermal diffusion. In this view, there is higher thermal conduction for $Pr < 1$. However, in cases where $Pr > 1$, such as in the case of water and engine oil, a low thermal conductivity is found, and in this scenario, as Pr increases, the thermal boundary layer reduces in thickness, resulting in a reduction in thermal diffusivity and a fall in the surface temperature, which leads to a higher heat transfer. This clearly demonstrates that with higher values of Pr, there is a decline in the Casson nanofluid temperature caused by the fact that there is a thinner thermal structure. Thus, for improving heat transmission processes and cooling enhancement in the Casson nanofluid, Pr can be incorporated. On the other hand, rising values of Q and Nr lead to thickening of the thermal boundary structure, and such a reaction reduces heat transfer across the surface.

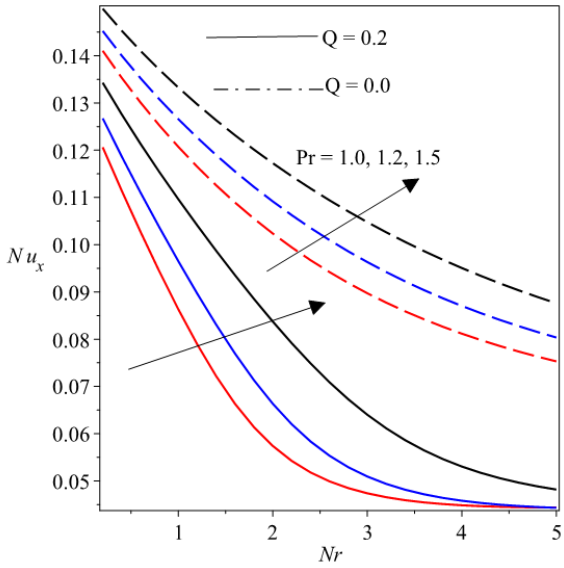

Figure 12 Nu_x for variations in Q, Pr and Nr

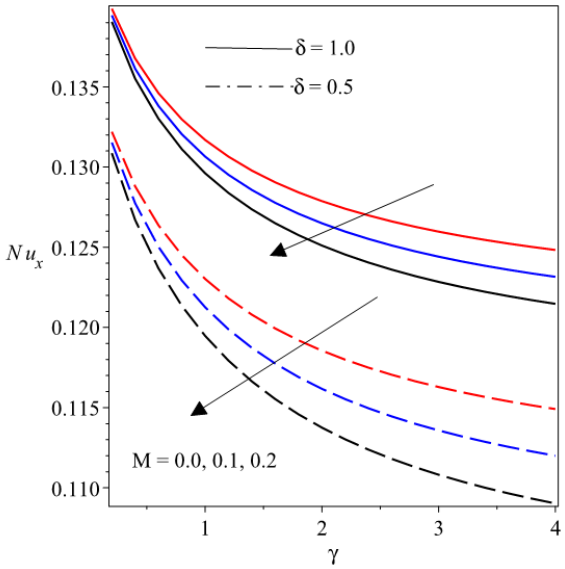

Figure 13 Nux for variations in M, δ and δ

In Figure 13, there is a depreciation in the surface heat transfer as M and γ enhance in strength, but the opposite reaction occurs with the escalating nature of the power-law index δ. The reasons for these observations are that a thickened thermal boundary structure is produced when M and γ increase and as such, heat transfer is impeded, which leads to a fall in Nu_x. Conversely, a thin structure of thermal film is generated due to growing values of δ, as such, surface temperature falls, and thus, heat transfer improves significantly, as found in figure 13.

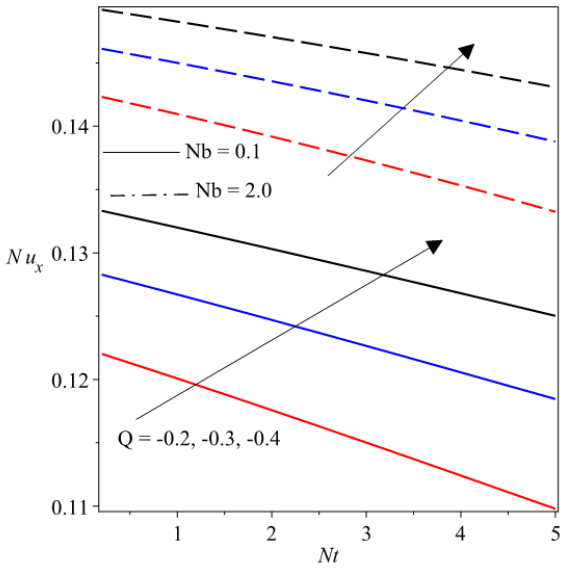

Figure 14 Nu_x for variations in $Nb, (-Q)$ and Nt

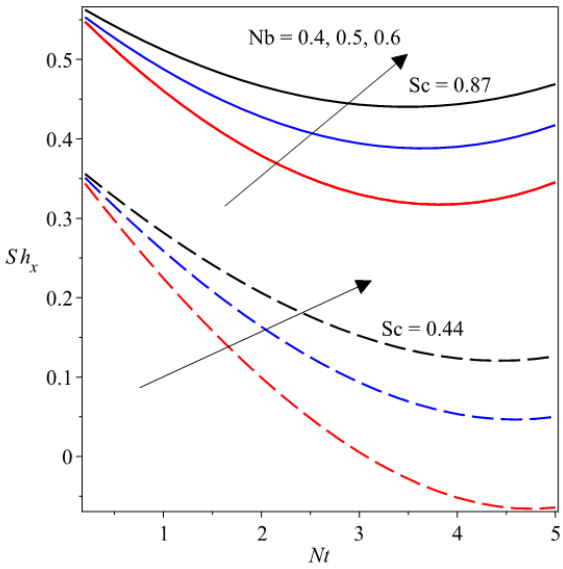

Figure 15 Sh_x for variations in Sc, Nb and Nt

Owing to the magnification of the Brownian motion in the thermal field, there is a rise in Nu_x as observed in figure 14. Likewise, the effects of the heat sink Q is to enhance Nu_x due to a reduction in the temperature distribution. The thermophoresis term, which is indicated as Nt is inversely proportional to the trend of Nu_x due to the fact that magnifying the strength of Nt is responsible for a thickening of the thermal boundary structure. In such a case, heat transfer is impeded across the sheet surface. In figure 15, it is observed that the mass transfer improves with the escalating values of the Schmidt number Sc and Brownian motion term Nb whereas there is a depletion in the

profiles of the mass transfer as the thermophoresis term increases.

Conclusions

In the current study, a numerical model is developed to analyze the thermal behaviour of a Casson fluid experiencing some tiny particles over a device that extends nonlinearly in dual directions and is conditioned by convective heating at the thermal wall. The mathematical model that depicts the three-dimensional flow is set up in the presence of the magnetic field effect using the Buongiorno model, consisting of the thermophoresis and Brownian motion terms in the transport phenomenon. A numerical solution was sought for the formulated governing equations, and the results were publicized using various graphs to showcase the behaviour of the emerging physical terms in the flow regime. In the analysis, it has been found that:

- Heat transmission of the Casson nanofluid is an increasing function of the power-law index δ, the Prandtl number Pr and heat sink parameters but a decreasing function of the thermophoresis Nt, magnetic field M, radiation Nr and heat source terms.
- There is a temperature upsurge in the thermal profile as the Casson material term, heat source, and radiation parameters escalate in strength, but a lower thermal profile results from the higher magnitude of the power-law index δ.
- Wall frictional drag increases in both directions with escalating values of the magnetic field, Casson material, and power-law exponent terms, but a thinning hydrodynamic boundary layer developed with growth in γ and δ.
- The mass transfer increases with the enhancement of the Schmidt number Sc, Brownian motion term Nb but the impact of the thermo-migrating tiny particles prevents a rise in the mass transfer.

The results from this study finds is found useful in engineering and industrial works involving high-temperature operations, like metal casting, hot rolling, glass manufacturing, etc. Application of this knowledge can promote energy savings and improved product quality. The current study can also be extended to the case of variable thermophysical properties and the study of some other non-Newtonian fluids, such as the micropolar fluids, Jefferey, Williamson, Prandtl-Eyring, etc.

References

Abbas, Z. S., Khan, W. A., Gulzar, M. M., Hayt, T., Waqas, M and Asghar, Z. (2020). Magnetic field influence in three-dimensional rotating micropolar nanoliquid with convective conditions, Computer Methods and Programs in Biomedicine, 189, 105324.

Choi, S.U.S. (1995). Enhancing thermal conductivity of fluids with nanoparticles, USA, ASME, FED 231/MD 66, 99–105.

Das, S., Mondal, H., Kundu, P. K. and Sibanda, P. (2018). Spectral quasilinearization method for Casson fluid with homogeneous heterogeneous reaction in presence of nonlinear thermal radiation over an exponential stretching sheet, Multidiscipline Modeling in Materials and Structures, 1-20, doi.org/10.1108/MMMS-04-2018-0073

Devi, S.P.A. and Thiyagarajan, M. (2006). Steady nonlinear hydromagnetic flow and heat transfer over a stretching surface with variable temperature, Heat Mass Transfer, 42, 671-677, doi.org/10.1007/s00231-005-0640-y.

Devi, S. P. A. and Prakash, M. (2015). Temperature dependent viscosity and thermal conductivity effects on hydromagnetic flow over a slendering stretching sheet, Journal of the Nigerian Mathematical Society, 34, 318–330.

Fatunmbi, E. O. and Okoya, S. S. (2020). Heat Transfer in Boundary Layer Magneto-Micropolar Fluids with Temperature-Dependent Material Properties over a Stretching Sheet, Advances in Materials Science and Engineering, 2020, 1-11, https://doi.org/10.1155/2020/5734979

Fatunmbi, E. O. and Okoya, S. S. (2021). Quadratic Mixed Convection Stagnation-Point Flow in Hydromagnetic Casson Nanofluid over a Nonlinear Stretching Sheet with Variable Thermal Conductivity, Defect and Diffusion, 409, 95-109.

Javed, T., and Siddiqui, M. A. (2018). Energy transfer through mixed convection within square enclosure containing micropolar fluid with non-uniformly heated bottom wall under the MHD impact, J. Mol. Liq. 249, 831–842.

Khan J. A, Mustafa, M., Hayat, T., Alsaedi, A. (2014). On Three-Dimensional Flow and Heat Transfer over a Non-Linearly Stretching Sheet: Analytical and Numerical Solutions, PLoS ONE 9(9), e107287. doi: 10.1371/journal.pone.0107287

Khan, J. A., Mustaf, M., Hayat, T. Alsaedi, A. (2015). Three-dimensional flow of nanofluid over a non-linearly stretching sheet: An application to solar energy, International Journal of Heat and Mass Transfer, 86, 158–164.

Krishna, Y. H., Reddy, G. V. R. and O.D. Makinde, O. D. (2018). Chemical Reaction Effect on MHD Flow of Casson Fluid with Porous Stretching Sheet, Defect and Diffusion Forum, 389, 100-109.

Laha, M. K., Gupta, P. S. and Gupta, A. S. (1989). Heat transfer characteristics of the flow of an incompressible viscous fluid over a stretching sheet, Wfirme-und Stofffibertragung, 24, 151-153.

Liu, I. and Andersson, H. I. (2008). Heat transfer over a bidirectional stretching sheet with variable thermal conditions, International Journal of Heat and Mass Transfer, 51, 4018–4024.

Matin, M. H, Dehsara, M. and Abbassi, A. (2012). Mixed convection MHD flow of nanofluid over a non-linear stretching sheet with effects of viscous dissipation and variable magnetic field, Mechanika, 18(4), 415-423.

Omotola, O. E. and Fatunmbi, E. O. (2021). Dynamics of Multiple Slip and Thermal Radiation on Hydromagnetic Casson Nanofluid Flow over a Nonlinear Porous Stretchable Surface, Physical Science International Journal, 25(4): 1-14.

Patel, H.R. and Singh, R. (2019). Thermophoresis, Brownian motion and non-linear thermal radiation effects on mixed convection MHD micropolar fluid flow due to nonlinear stretched sheet in porous medium with viscous dissipation, joule heating and convective boundary condition, Int. Commun. Heat Mass Transfer 107, 68–92

Pramanik, S. (2013). Casson fluid flow and heat transfer past an exponentially porous stretching surface in presence of thermal radiation, Ain Shams Eng J, 2013, http://dx.doi.org/10.1016/j.asej.2013.05.003

Salahuddin, T. Arshad, M. A., Siddique, M., Alqahtani, A.S. and Malik, M. Y. (2020). Thermophysical properties and internal energy change in Casson fluid flow along with activation energy, Ain Shams Engineering Journal, 11, 1355–1365.

Shit, G. C. and Mandal, S. (2020). Entropy Analysis on Unsteady MHD Flow of Casson Nanofluid over a Stretching Vertical Plate with Thermal Radiation Effect, Int. J. Appl. Comput. Math, 6(2), doi.org/10.1007/s40819-019-0754-4

Sreenivasulu P. Poornima, T. and Reddy. N. B. (2016). Thermal Radiation Effects on MHD Boundary Layer Slip Flow Past a permeable Exponential Stretching Sheet in the Presence of Joule Heating and Viscous Dissipation, Journal of Applied Fluid Mechanics, 9(1), 267-278, 2016.

Sreenivasulu, P. Poornima, T. and Reddy, N. B. (2019). Influence of Joule Heating and Non-Linear Radiation on MHD 3D Dissipating Flow of Casson Nanofluid past a Non-Linear Stretching Sheet, Nonlinear Engineering, 8, 661–672.

Vajravelu, K., Prasad, K. V, Vaidya, H., Basha, N. Z., Chiu-On Ng. (2016). Mixed Convective Flow of a Casson Fluid over a Vertical Stretching Sheet, Int. J. Appl. Comput. Math DOI 10.1007/s40819-016-0203-6

Zeeshan, A. and Majeed, A. (2016). Heat transfer analysis of Jeffery fluid flow over a stretching sheet with suction/injection and magnetic dipole effect, Alexandria Eng. J. (2016), http://dx.doi.org/10.1016/j.aej.2016.06.014

Sheri, S and Shamshuddin, MD. (2018). Finite element analysis on transient magnetohydrodynamic (MHD) free convective chemically reacting micropolar fluid flow past a vertical porous plate with Hall current and viscous dissipation, Propul Power Res. 7 (2018) 353–365.

Zubair, M., Waqas, M., Hayat, T., Ayub, M and Alsaedi, A. (2017). The onset of modified Fourier and Fick's theories in temperature-dependent conductivity flow of micropolar liquid, Results Phys. 7 (2017) 3145–3152.